Digest Journal of Nanomaterials and Biostructures Vol. 20, No. 4, October-December 2025, p. 1487-1498

Theoretical study of physical characterization of ScP and ScAs binary compounds and their ternary alloy $ScP_{1-x}As_x$: Wien2K code

N. Meneceur [a], Y. Megdoud [b,c] , R. Meneceur [a], A. Boukhari [a],
Y. Benkrima [d*], L. Tairi [e], M. Laouamer [a], H. Bouraoui [f]
[a] *Unit for the Development of Renewable Energies in Arid Zones (UDERZA), El Oued University, Algeria*
[b] *Institute of Sciences, Centre University of Tipaza, Algeria,*
[c] *LPR Laboratory, Département of Physics, Faculty of Science, Badji Mokhtar University, Annaba, Algeria.*
[d] *Ecole Normale Superieure de Ouargla 30000 Algeria*
[e] *Research Center in Industrial Technologies CRTI, P.O. Box 64, Cheraga16014 Algiers Algeria*
[f] *Faculty of Hydrocarbons, Renewable Energies, Earth and Universe Sciences, Kasdi Merbah – Ouargla University, Ouargla 30000, Algeria*

The study investigates the ternary alloy ($ScP_{1-x}As_x$) and delves into its structural, electronic, and optical characteristics across various compositions. Employing density functional theory (DFT) calculations utilizing the FP-LAPW+lo method within the WIEN2k computational package, the researchers initially focus on the alloy's phase stability. Results reveal that the alloy maintains stability within a NaCl crystal structure across all compositions examined. Furthermore. The findings suggest promising absorption coefficients and optical bandgaps, indicating the potential suitability of the alloy for optoelectronic device applications. This implies that the ($ScP_{1-x}As_x$) ternary alloy could hold promise in the development of various optoelectronic devices, leveraging its structural and optical properties for enhanced performance in relevant applications.

(Received September 12, 2025; Accepted December 2, 2025)

Keywords: Density functional theory DFT, FP-LAPW method, mBj, Band-gap, Optical properties, Wc-GGA

1. Introduction

The passage provides a comprehensive overview of the recent surge in interest in Scandium III–V based materials, focusing on the anomalous physical properties observed across structural, magnetic, and phonon characteristics. Researchers have conducted extensive investigations into the bulk properties of scandium pnictides, encompassing various aspects such as Fundamental properties. These studies have been conducted using a combination of experimental and theoretical methods, as referenced in [1–13].

Despite the comprehensive exploration of many properties of these materials, the phonon properties of ScN have received relatively little attention, with only a few studies dedicated to their investigation [14]. This discrepancy highlights a potential gap in our understanding of the vibrational dynamics and lattice vibrations of ScN, emphasizing the need for further research in this area. Addressing this gap could provide valuable insights into the thermal and mechanical behavior of ScN, crucial for understanding its overall stability and performance in practical applications. Additionally, a deeper understanding of ScN's phonon properties could contribute to the development of new materials with tailored thermal and mechanical characteristics, potentially advancing fields such as thermoelectrics, phononics, and materials engineering.

Furthermore, the passage discusses the use of first-principle electronic band structure calculations to study the properties of scandium III–V based materials. These calculations reveal multi-overlap lines between valence and conduction bands, indicating metallic behavior. This observation has been emphasized by the authors, suggesting that the materials exhibit metallic

* Corresponding author: b-amina1@hotmail.fr
https://doi.org/10.15251/DJNB.2025.204.1487

characteristics. The consistency of these results across different studies, as evidenced by findings from another reference, Ref. [13], underscores the robustness of the findings and strengthens our understanding of the electronic properties of scandium III–V based materials.

Finally, the passage acknowledges the progress made in understanding the structural and electronic properties of ScP and ScAs compounds through theoretical frameworks but points out a significant gap in our comprehension regarding their dynamic properties, specifically their phonon characteristics. Understanding the phonon properties of ScP and ScAs is crucial due to their influence on various physical attributes of solids, including phase transition phenomena, thermodynamic stability, and a range of transport and thermal properties. Therefore, a deeper comprehension of these compounds' phonon properties is essential for accurately predicting and manipulating their behavior across diverse applications in materials science and engineering.

The present work provides a structured overview of an article focusing on the computational investigation of the physical properties of ternary alloys ScP1−xAsx, as well as their binary compounds ScP and ScAs. Here's a breakdown of the outlined structure:

- **Section 2: Computational Details**

This section presents an overview of the computational methodologies utilized in the study. It likely includes descriptions of the software packages, algorithms, and theoretical frameworks employed to conduct the calculations. This part sets the foundation for the subsequent analysis and interpretation of results.

- **Section 3: Results and Discussions**

In this section, the findings from the computational calculations are elaborated upon and discussed. It covers a range of physical properties of the ternary alloys and binary compounds, such as their electronic structure, bandgap characteristics, lattice dynamics, and potentially other relevant attributes. Discussions may delve into the implications of these findings, their alignment with existing theories or experimental data, and potential applications in various fields.

- **Concluding Section**

In this part, we present the results and conclusions and discuss them. It encapsulates the contributions made to understanding the physical properties of the materials under investigation. Additionally, it may offer insights into potential future research directions and avenues for further exploration in the field.

The structured format of the article facilitates easy navigation for readers, guiding them through the computational methodology, presentation of results, and the overarching conclusions. This organization ensures clarity and coherence in conveying the study's objectives, findings, and implications to the audience.

2. Theoretical details

The study utilized density functional theory (DFT) [15,16], to comprehensively analyze the physical properties of ScP and ScAs compounds, as well as their alloys $ScP_{1-x}As_x$. Specifically, the augmented plane wave (FP-LAPW) [17, 18], method implemented within the Wien2k code [19] was employed for calculations. The generalized gradient approximation for exchange and correlation interactions. For exchange and correlation interactions we used the generalized gradient approximation, following the Wu and Cohen (WC-GGA) scheme [20], was utilized to accurately determine total energy and electronic properties. To address the GGA [20] underestimation of the band gap, the Tran and Blaha-modified Becke-Johnson potential (mBJ) was incorporated for electronic property calculations. Wave function expansion within the atomic sphere was conducted with a maximum value of angular momentum (l_{max}=10). A plane wave expansion in the interstitial region with RMTKmax was chosen, with a value of seven across all investigated systems. The Fourier expansion of the potential and charge density utilized $G_{max} = 12\ (Ry)^{1/2}$. Specific muffin-tin radii (R_{MT}) were assigned for each element: 2.2 for Sc, 1.8 for P and 2.09 for As, (all in atomic units). To integrate inside the Brillouin zone (BZ), the modified tetrahedron method was applied

with a dense mesh of 1000 k-points, ensuring convergence of total energy to less than 10^{-6} Ry. These meticulous computational parameters were crucial for accurately predicting the properties of the studied systems, providing valuable insights into their behavior at the atomic and electronic levels.

3. Results interpretation

3.1. Structural characterization

In this part, our main objective is to compute the total energies for $ScP_{1-x}As_x$ at different volumes. Figures 1 show case the total energy plotted against volume for both binary compounds and their ternary alloys in the NaCl phase. These graphical representations provide significant insights into the stability and energetic attributes of the systems under scrutiny. Our analysis of these plots aims to differentiate the relative stability among various compositions and identify the ideal conditions necessary for achieving the desired material properties.

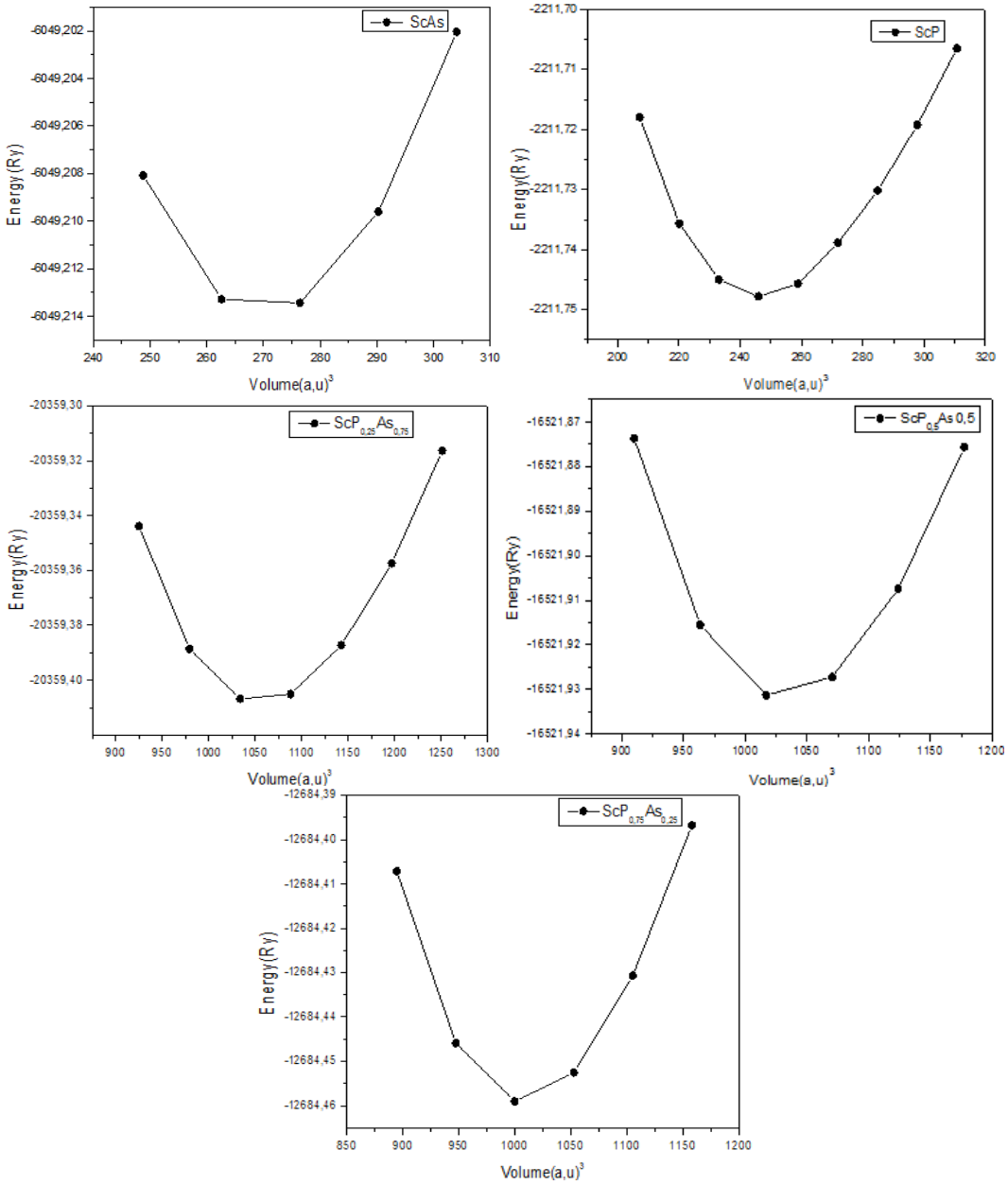

Fig. 1. Variation of total energy as a function of volume for ScAs, $ScP_{0.25}As_{0,75}$, $ScP_{0.5}As_{0.5}$, $ScP_{0,75}As_{0,25}$ and ScP in NaCl phase.

Continuing onward, we've employed the NaCl phase to ascertain the ground state properties of the materials. It's important to highlight that the system's stability diminishes with rising concentrations of phosphorus and arsenic. Subsequently, the total energies obtained are subjected to fitting with Murnaghan's equation of state [21] to extract structural properties, including lattice constants (a_0) and the bulk modulus (B_0) (Table 1) presents a succinct summary of the structural outcomes for the studied materials, juxtaposed with previous theoretical [25] and experimental works [22]. Moreover, the calculated lattice parameters for various compositions of $ScP_{1-x}As_x$ alloys suggest a tendency toward Vegard's law [23], with a slight upward bowing parameter evident in Fig. 5. The minor deviation from Vegard's law primarily stems from subtle mismatches in lattice parameters among the binary compounds ScP and ScAs. Notably, deviations from Vegard's law have been observed in semiconductor alloys, supported by both experimental observations [24] and theoretical considerations [25]. The overall trend in the variation of bulk modulus concerning the composition (x) for $ScP_{1-x}As_x$ ternary mixed crystals is illustrated in Fig. 6. When comparing the structural parameters of these materials (as shown in Figs. 6 and 7), a consistent pattern emerges: an increase in the lattice constant corresponds to a decrease in the bulk modulus. This alignment conforms to the established relationship between bulk modulus and lattice constant, represented by $B \propto V_0^{-1}$, where V_0 denotes the primitive cell volume.

Table 1. Value of Lattice parameter (A^0) of ScP_xAs_{1-x} in NaCl.

Materials	Compositions	Lattice parameter a(A^0)	Ref
ScAs	**0.00**	**5.761**	**[27]**
$ScP_{0.25}As_{0.75}$	**0.25**	**5.741**	
$ScP_{0.5}As_{0.5}$	**0.5**	**5.647**	
$ScP_{0.75}As_{0.25}$	**0.75**	**5.582**	
ScP	**1.00**	**5.523**	**[27]**

3.2. Electronic Band Structure Analysis

This passage discusses a study focusing on the energy bandgap in semiconductors, particularly ternary alloys of $ScP_{1-x}As_x$ with a rocksalt crystal structure. The researchers calculated the energy bandgap and electronic band structures using theoretical lattice parameters and the mBJ exchange potential.

For binary compounds ScP and ScAs, The minimum of the conduction band is located at point X the point Γ corresponds to the maximum of the valence band, therefore presents an indirect semiconductor.(Fig 2).

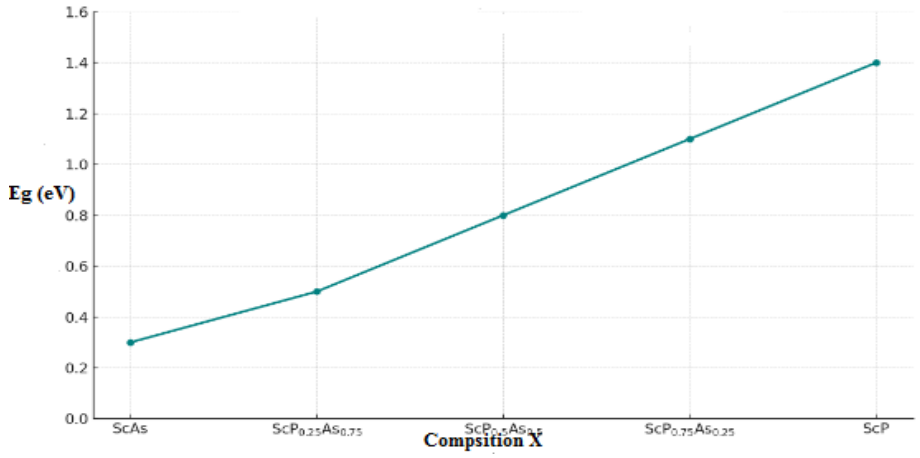

Fig. 2. Variation of the energy band gap values for ScP_xAs_{1-x} as a function of composition X.

However, in ternary alloys, both the conduction and valence band extrema are at the Γ point, suggesting a direct bandgap semiconductor nature. Results in table2.

Table 2. Value of gap (eV) of ScP_xAs_{1-x} in NaCl phase with Mbj Method.

Materials	Types of gap	Gap Value (mBj) (eV)	Ref
ScAs	Indirect (X-Γ)	0.431	[26]
$ScP_{0.25}As_{0.75}$	Indirect (X-Γ)	0.662	
$ScP_{0.5}As_{0.5}$	Indirect (X-Γ)	0.987	
$ScP_{0.75}As_{0.25}$	Indirect (X-Γ)	1.223	
ScP	Indirect (X-Γ)	1.524	[26]

Comparing their results with previous experimental and theoretical studies, the authors found good agreement, although their results were slightly lower than some reported values.

The study utilized the mBJ approximation method [20] , which yielded results consistent with other methodologies like GGA + USIC and GW[26], although some differences were noted compared to certain previously reported results.

Furthermore, the researchers observed that increasing the concentration of yttrium in the alloy compositions led to an increase in the bandgap, as depicted in the provided figures.

Overall, this research provides valuable insights into the energy bandgap and electronic properties of ternary alloys, which are essential for designing semiconductor materials for practical applications in electronic devices.

3.3. Optical characterizations

The optical properties of a materials are commonly expressed of the complex dielectric function $\epsilon(\omega)$, where: $\varepsilon(\omega) = \varepsilon_1(\omega) + i\varepsilon_2(\omega)$ [27].

Here:

$\varepsilon_1(\omega)$: (ω) represents the real part of the dielectric function, present the material's response in terms of polarization.

$\varepsilon_2(\omega)$: represents the imaginary part of the dielectric function, associated with the absorption of light and energy dissipation within the material.

The dielectric function provides essential information about how a material interacts with electromagnetic radiation across different frequencies (ω) [28-30]. It plays a critical role in understanding various optical properties of solids, including absorption, reflection, transmission, and dispersion.

In semiconductor physics, the energy band structure plays a fundamental role in determining the optical and electronic properties of the material. The refractive index, typically denoted as $n(\omega)$, where ω represents the angular frequency of light, is intimately linked to this band structure. In general, the refractive index can be related to the energy band structure through various models. One common approach is through the Sellmeier equation, which describes the refractive index of a material as a function of wavelength or frequency. However, for semiconductors, especially those with complex band structures, more sophisticated models may be required. [31- 33].

Commonly employed models include:

Sellmeier Equation: A phenomenological equation that presente $n(\omega)$, as a function of wavelength or frequency. It typically involves fitting experimental data to a sum of terms with coefficients called Sellmeier coefficients.

Wemple-Didomenico Model: This model connects the refractive index with the energy gap in semiconductors. It provides a relation between the refractive index and the energy gap based on the complex dielectric function and the energy band structure.

Single Oscillator Model: A simple model that assumes a single electronic oscillator and relates the refractive index to the energy gap. It provides a straightforward way to understand the optical properties of semiconductors but may lack accuracy for complex materials.

Effective Mass Approximation: In this model, the energy band structure near the band edge is approximated by a parabolic dispersion relation. The refractive index can be related to the effective mass of charge carriers and the energy gap.

These models offer different levels of complexity and accuracy in describing the relationship between the refractive index and the energy gap of semiconductors, making them valuable tools for understanding and predicting optical properties in various semiconductor materials.

The provided description outlines the optical characteristics of various materials, including binary compounds (ScP and ScAs) and their ternary alloys ($ScP_{1-x}As_x$) across different compositions. Here's a summary of the key findings:

The passage discusses the calculation of optical properties such as the dielectric constant, refractive index, and others for both the material ($ScP_{1-x}As_x$) using the mBJ approximation. Here's a breakdown of the information provided:

Scope of the Study: The study focuses on assessing the optical behavior of ($ScP_{1-x}As_x$) alloys across a range of energy from 0 to 40 eV. This assessment is conducted through calculations of various optical parameters.

Representation of Results: The obtained results are presented in Figures 3 - 7 These figures depict the response of different optical properties as a function of energy for different concentrations of x in ($ScP_{1-x}As_x$) alloys.

3.3.1. Dielectric Function ε2(ω)

Figure 3 displays the response of the imaginary part of the dielectric function (ε2(ω)) as a function of energy in the range of 0 to 40 eV for different concentrations of x. The curves for all concentrations exhibit similar qualitative behavior, starting from value (Zero) and gradually increasing from specific incident photon values.

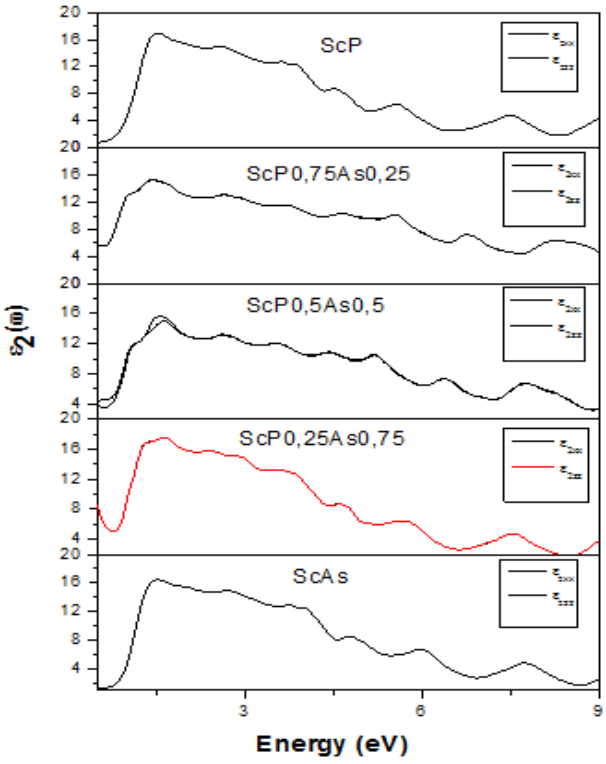

Fig. 3. Imaginary part of the dielectric function $\varepsilon_2(\omega)$ as a function of photon energy for $ScP_{1-x}As_x$ alloys with $x = 0, 0.25, 0.5, 0.75,$ and 1.

Optical Gap: The energy values at which the curves start increasing represent the optical gap corresponding to each composition of $ScP_{1-x}As_x$. These values are found to be consistent with electronic energy bandgaps, indicating agreement between optical and electronic properties.

Maximum Absorption: Each curve reaches a maximum value corresponding to specific energies for different concentrations of x. These maximum values indicate strong absorption of light photons, particularly in the ultraviolet region, for all concentrations of the alloys.

Applicability in Optoelectronics: The observed strong absorption of light photons in the (UV) region suggests the potential applicability of $ScP_{1-x}As_x$ alloys in optoelectronic devices.

Overall, the passage highlights the optical behavior of ScP1-xAsx alloys, indicating their potential utility in optoelectronic applications, particularly due to their strong absorption of light photons in the ultraviolet range.

3.3.2. The dielectric function ($\varepsilon_1(\omega)$)

This passage discusses the results obtained for ($\varepsilon 1(\omega)$) for $ScP_{1-x}As_x$ alloys over a range of incident photon energies from 0 to 40 eV. Here's a breakdown of the information provided:

Behavior of $\varepsilon 1(\omega)$: The curves representing $\varepsilon 1(\omega)$ for different concentrations of x exhibit similar qualitative behavior in Fig. 4. They start from $\varepsilon 1(\omega = 0)$ and gradually increase until they reach maximum peak values at specific energies for each concentration. These peak values are reported for each concentration, and their agreement with previously reported results is noted.

Dispersion and Absorption: At certain energy values, the dispersion is zero, indicating maximum absorption. Beyond this, $\varepsilon_1(\omega)$ starts to decrease and reaches negative minimum values, suggesting metallic behavior in the energy range of (9.428–13.183) eV. This indicates a reflection of incident light photons within this energy range. The results align with previously reported findings within the interval of (9.90 to 13.4 eV).

Positive Results: After the negative region, $\varepsilon_1(\omega)$ becomes positive for specific energy values corresponding to each concentration of P These positive values are reported for x = 0, 0.25, 0.5, 0.75, and 1.

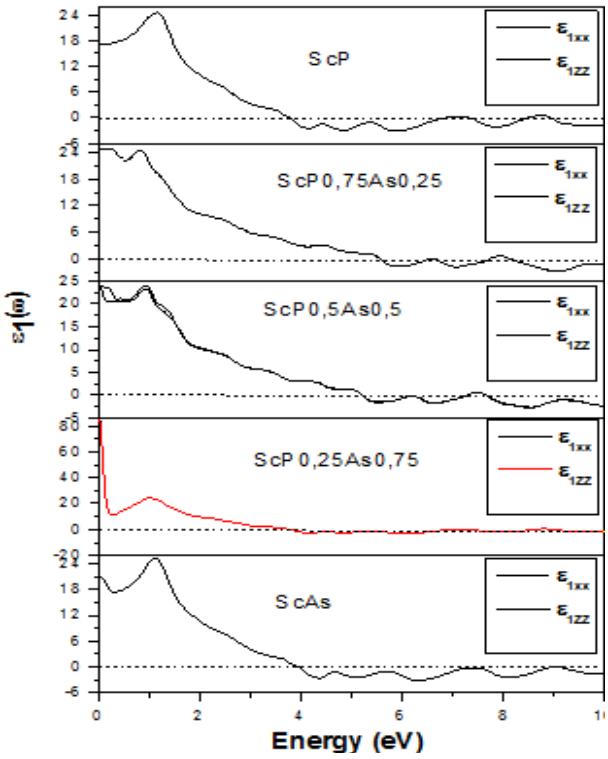

Fig. 4. Real part of the dielectric function $\varepsilon_1(\omega)$ plotted as a function of photon energy for $ScP_{1-x}As_x$ with $x = 0, 0.25, 0.5, 0.75,$ and 1.

Comparison with Theoretical Models: Static values of $\varepsilon_1(\omega)$ corresponding $\omega=0$, along with results from other theoretical study , are presented in Table 7. The obtained results for $\varepsilon 1(0)$ are noted to be somewhat lower than those obtained by other theoretical models across all concentrations of P.

Relation with Bandgap Energy: Figure 9 illustrates the results of $\varepsilon_1(0)$ as a function of P concentration and energy bandgap. It's observed that $\varepsilon_1(0)$ decreases with increasing concentration of P and bandgap energy values, which aligns with Penn's model, indicating an inverse relation between $\varepsilon_1(0)$ and bandgap energy.

Overall, the passage provides detailed insights into the behavior of the real part of the dielectric function for ScP_{1-x} As_x alloys, including its dispersion, absorption characteristics, comparison with theoretical models, and relation with bandgap energy.

3.2.3. The refractive index (n(ω))

This passage elaborates on the results obtained for the refractive index (n(ω)) as a function of energy for (ScP1-xAsx) alloys within the energy interval of 0 to 40 eV. Here's a breakdown of the provided information:

Representation of Results: The results for n(ω) are depicted in Figure 5 for all suggested concentrations of ScP_{1-x} As_x alloys. It's noted that all curves in the figure start from corresponding values of n(0) at zero energy and gradually increase, reaching maximum values at specific energies for each composition.

Maximum Values of n(ω): The maximum values of n(ω) correspond to specific energies for each concentration of ScP_{1-x} As_x

Comparison with Previous Literature: The obtained results are claimed to be superior to those reported in previous literature [43]. This suggests an advancement or improvement in the accuracy or reliability of the calculated refractive indices.

Decreasing Trend: After reaching their maximum values, the results of n(ω) start to decrease. This likely indicates a reduction in refractive index beyond certain energy levels.

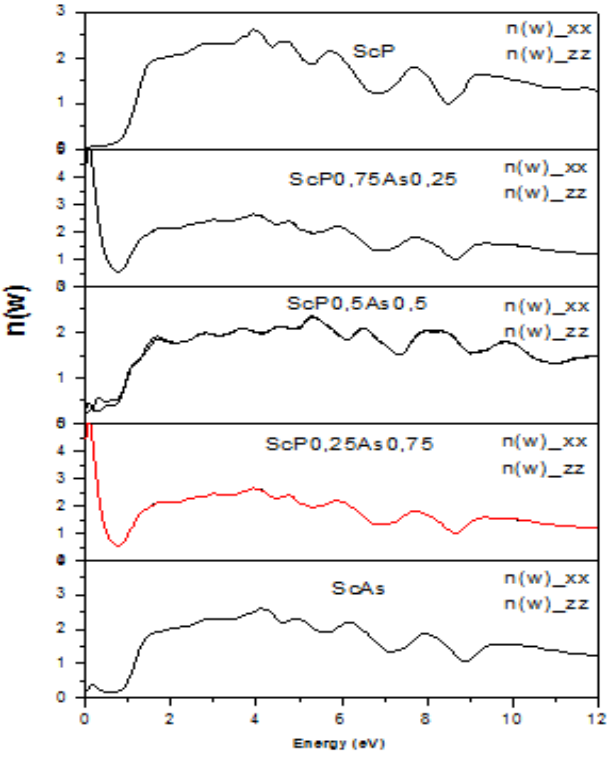

Fig. 5. Refractive index $n(\omega)$ *as a function of photon energy for the* $ScP_{1-x}As_x$ *alloy system at different compositions.*

Comparison with Moss Model: It is mentioned that the value obtained using the Moss model produced better results than the FP-L(APW + lo) method. This comparison likely emphasizes the agreement or similarity between the findings obtained from different theoretical models.

Static Refractive Index (n(0)): The static values of (n(0)) and other computed results are presented in (Table 3) . Additionally, these value are depicted as a function of P concentration and energy of interdit band values in Figure 10.

Overall, the passage provides insights into the behavior of the refractive index for $ScP_{1-x}As_x$ alloys, highlighting maximum values, comparison with previous literature, and the agreement between different theoretical models.

3.2.4. The absorption characteristics and reflectivity spectra

This passage discusses the absorption characteristics and reflectivity spectra of ternary alloys $ScP_{1-x}As_x$ within the energy range of 0 to 40 eV:

Absorption Coefficients: In Figure 6, the results of the coefficients of absorption with respect to incident photon energy are presented. It is observed that all curves exhibit similar behavior. The fundamental absorption threshold initiates at specific energies for each concentration of $ScP_{1-x}As_x$, namely 0.884 eV, 0.966 eV, 1.179 eV, and 1.183 eV. These thresholds align well with the energies of the electronic energy bandgaps, indicating consistency between absorption behavior and bandgap energies.

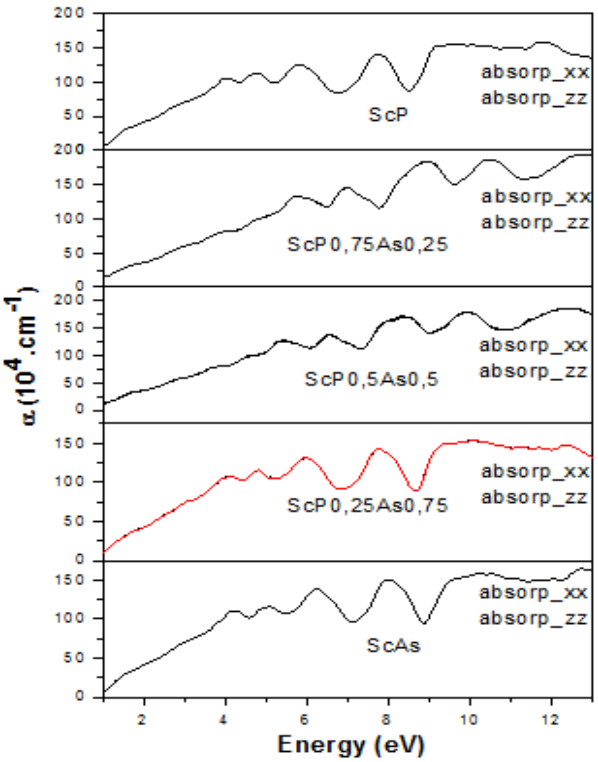

Fig. 6. Absorption coefficient $\alpha(\omega)$ as a function of photon energy for $ScP_{1-x}As_x$ alloys with $x = 0, 0.25, 0.5, 0.75,$ and 1.

Maximum Absorption Energies: The results corresponding to the energies of maximum absorption are collected in Table 3. These findings suggest that $ScP_{1-x}As_x$ alloys demonstrate absorption primarily in the ultraviolet range, suggesting potential applications in optoelectronics.

Reflectivity Spectra: The reflectivity spectra of ScP1-xAsx alloys are depicted in Figure 7. It's noted that the curves are similar for all values of x, indicating consistent behavior across different alloy compositions.

Reflectivity at Zero Frequency (R(0)): Table 3 presents the results obtained for the reflectivity result of the alloy at zero frequency, denoted as R(0). This parameter provides insight into the material's reflective properties under static conditions.

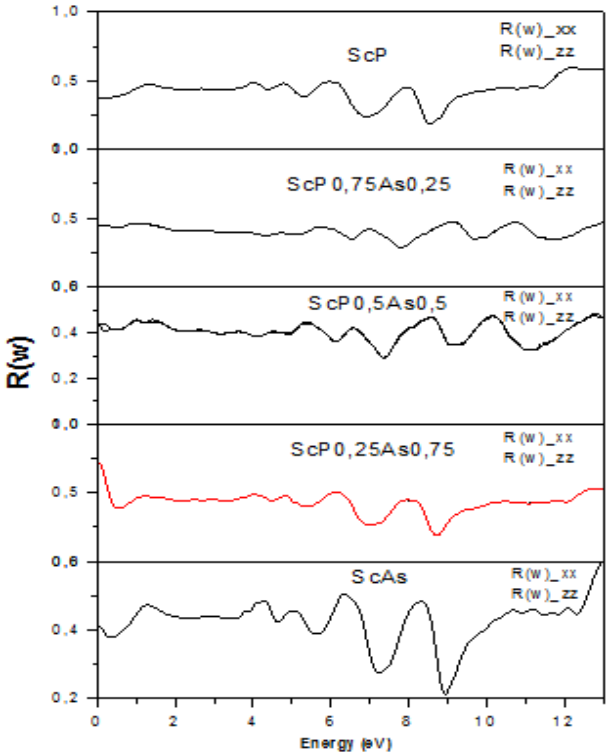

Fig. 7. Reflectivity as a function of photon energy for the ScPAs alloy at $(x = 0, 0.25, 0.5, 0.75$ *and* $1)$.

Overall, the passage provides a comprehensive overview of the absorption and reflectivity characteristics of $ScP_{1-x}As_x$ alloys, highlighting their potential for applications in optoelectronics and the consistency of results across different alloy compositions

Table 3. Estimated Optical Properties (NaCl Phase)for ScP_xAs_{1-x}.

Material	Composition	Relative index n_0	Static Dielectric Constant e_0
ScAs	X=1	4.52	20
$ScP_{0.25}As_{0.75}$	X=0.75	4.33	17
$ScP_{0.5}As_{0.5}$	X=0.5	4.01	15
$ScP_{0.75}As_{0.25}$	X=0.25	3.75	12
ScP	X=0	3.42	10

Table 3 shows that the values of R(0), representing reflectivity at zero frequency, decrease as the concentration of As increases. This suggests that as the concentration of As increases, the electronic energy bandgap of the material increases, leading to a decrease in reflectivity. Additionally, Table 3 collects the values of maximum reflectivity, providing further insight into the reflective properties of the material across different compositions.

4. Conclusion

During this study, we studied the physical properties of the binary compounds ScP and ScAs and $ScP_{1-x}As_x$ alloy. We used the ab-initio method within the framework of density functional theory (DFT).

The structural results presented the lattice parameter and the compressibility modulus for the compounds ScP and ScAs and the allpy $ScP_{1-x}As_x$. The calculated values of the gaps of these materials using (WC-GGA) and (mBj). The optical properties. We have determined the complex dielectric function and the refractive index. The results obtained are in good agreement with those of other theoretical calculations.

References

[1] C. Stampfl, R. Asashi, A. J. Freeman, Phys. Rev. B 65, 161204-1 (2002); https://doi.org/10.1017/CBO9780511754647
[2] W. R. Lambrecht, Phys. Rev. B 62, 13538 (2000); https://doi.org/10.1063/1.3600702
[3] N. Takeuchi, Phys. Rev. B 65, 045204-1 (2002); https://doi.org/10.1016/S1369-7021(07)70275-4
[4] N. Takeuchi, S. U. Uloa, Phys. Rev. B 65, 235307-1 (2002); http://dx.doi.org/10.1002/9780470974704.ch1
[5] F. Tientega, J. F. Harrison, Chem. Phys. Lett. 223, 202 (1994); https://doi.org/10.1002/pip.1021
[6] J. Hayashi, I. Shirotani, K. Hirano, N. Ishimasu, O. Shimomura, T. Kikegaw, Solid State Commun. 125,543 (2003); http://dx.doi.org/10.1016/j.jssc.2004.07.020
[7] A. G. Petukhov, W. R. Lambrecht, B. Segall, Phys. Rev. B 50, 7800 (1994); https://doi.org/10.1051/jp420020021
[8] S. Y. Savrasov, Phys. Rev. B 54, 16470 (1996); https://doi.org/10.3390/coatings12111778
[9] S. H. Vosko, L. Wilk, M. Nussair, Can. J. Phys. 58, 1200 (1980); https://doi.org/10.1016/0022-3697(70)90234-9.
[10] Seraphin B. O.) Hess R. B., Phys. Rev. Lett. 14, 138. (1965); https://doi.org/10.1103/PhysRevLett.14.138.
[11] O. K. Andersen, Phys. Rev. B 13, 3050 (1975); https://doi.org/10.1103/PhysRev.93.632.
[12] N. Farrer and L. Bellaiche, Phys. Rev. B 66, 201203 (2002); https://doi.org/10.1016/j.jallcom.2019.153610.
[13] F. D. Murnaghan, Proc. Natl. Acad. Sci. (USA) 30, 5390 (1944); https://doi.org/10.1103/PhysRevB.64.195134
[14] F. Birch, Phys. Rev. 71, 809 (1947) https://doi.org/10.1016/S0010-4655(02)00206-0
[15] Hohenberg P, W. Kohn, Phys. Rev. B 136 (1964) 864; https://doi.org/10.1103/PhysRevB.75.115131
[16] Kohn W, Sham L J, Phys. Rev. A 140 (1965) 1133; https://doi.org/10.1103/PhysRevLett.102.226401
[17] Madsen G K H, Blaha P, Schwarz K, Sjostedt E, Nordstr€om L, Phys. Rev. B 64 (2001) 195134. https://doi.org/10.1063/1.354817
[18] Schwarz K, Blaha P, Madsen G K H, Comput. Phys. Commun. 147 (2002) 71 ; https://doi.org/10.1107/S0365110X58000827
[19] Blaha P, Schwarz K, Madsen GKH, Kvasnicka D, Luitz J, WIEN2k, An Augmented Plane Wave Plus Local Orbitals Program for Calculating Crystal Properties, Vienna University of Technology, Vienna, Austria, 2001; https://doi.org/10.1149/1.2424125
[20] Wu Z, Cohen R E, Phys. Rev. B 73 (2006) 235116; https://doi.org/10.1063/1.126058
[21] Murnaghan FD (1944) Proc Natl Acad Sci USA 30:244; https://doi.org/10.1103/PhysRevLett.12.538
[22] Abu Jafar MS, Abu Labdeh AM, El Hasan M (2010) Comput Mater Sci 50:269–273; https://doi.org/10.1016/0022-3697(68)90238-2

[23] Deng R, Ozsdolay BD, Zheng PY, Khare SV, Gall D (2015) Phys Rev B 91:045104; https://doi.org/10.1016/j.matchemphys.2017.06.009
[24] Saha B, Acharya J, Sands TD, Waghmare UV (2010) J Appl Phys 107:033715; https://doi.org/10.1103/PhysRevLett.102.226401
[25] Sukkabot W (2019), Physica B 570:236–240; https://doi.org/10.1016/j.infrared.2006.04.001
[26] Blanco MA, Martin Pendàs A, Francisco E, Recio JM, Franco R (1996), J Mol Struct Theochem 368:245; http://dx.doi.org/10.1007/s10853-014-8732-z
[27] Ravindra N M et al. 2007, Infrared Phys. Technol. 50 21 ; http://dx.doi.org/10.1063/1.370704
[28] Moss T S 1950, Proc. Phys. Soc. B 63 167 ; https://doi.org/10.1103/PhysRevLett.7.118
[29] Gupta V P, Ravindra N M 1980 Phys. Status Solidi B 100 715 ; https://doi.org/10.1016/j.mssp.2016.02.015.
[30] Ruoff A L 1984 Mater. Res. Soc. Symp. Proc. 22 287 ; https://doi.org/10.1016/S0925-3467(97)00171-7.
[31] Reddy R R et al. 1993, Infrared Phys. 34 103 ; https://doi.org/10.1016/j.commatsci.2009.11.030.
[32] Deligoz E, Colakoglu K, Ciftci Y O, Ozisik H, Journal of Physics and Chemistry of Solids, Vol. 68, Iss. 4, 482–489, April 2007; https://doi.org/10.48550/arXiv.1509.08246
[33] Daoud S, Lebga N, International Journal of Physical Research, 4(1), 1-5, 2016; https://doi.org/10.1016/j.physb.2004.03.087